Supporting information for: Rheology of Carbon Nanotube Networks During Gelation

D.T.N. Chen, K. Chen, L.A. Hough, M.F. Islam, A.G. Yodh*

Department of Physics and Astronomy, University of Pennsylvania, Philadelphia, PA, USA 19104-6396

E-mail: yodh@physics.upenn.edu

In the first part of the Supporting Information section, we present a detailed discussion of the correction for dynamic errors in the mean square displacement (MSD) data.

The dynamic error stems from the "smearing" of the particle image that results if the particle moves significantly during the time interval that the CCD camera's electronic shutter is integrating. The smearing affects the centroiding that the image processing algorithm uses to determine the position of the particle's center. The net effect of the dynamic error is to cause the apparent displacement of the tracked particle to be smaller than the actual displacement. This in turn results in mean square displacement $\langle \Delta x^2(\tau) \rangle$ with downward curvature at short lag time τ. Savin and Doyle[1] have carried out a detailed analysis of the dynamic error on the MSD and obtained a general formula, derived from convolving the particle displacement with a blur kernel, which yields an expression for the dynamic error-biased MSD:

$$\langle \Delta x^2(\tau,\sigma) \rangle = \frac{1}{\sigma^2} \int_0^\sigma [\langle \Delta x^2(\tau+\xi) \rangle + \langle \Delta x^2(\tau-\xi) \rangle - 2\langle \Delta x^2(\xi) \rangle](\sigma-\xi)d\xi. \qquad \text{(SA1)}$$

where σ is the shutter time. In theory, any functional form describing the MSD can be plugged into

*To whom correspondence should be addressed

Eq. (SA1) and a functional form for the dynamic error-biased MSD can be obtained. This is the basic procedure that we use for our MSD data. We first briefly demonstrate its use on experimental data for a relatively simple system - particle diffusion in a Newtonian fluid. In the absence of static and dynamic errors, the measured ensemble-averaged MSD will be described by the functional form: $\langle \Delta x^2(\tau) \rangle = 2D\tau$ where $D = k_b T/(6\pi\eta a)$ is the self-diffusion coefficient with temperature T, viscosity η, and particle radius a. However, in the presence of errors, the MSD becomes:

$$\langle \Delta x^2(\tau,\sigma) \rangle = 2D(\tau - \sigma/3) + 2\varepsilon^2. \tag{SA2}$$

where the first term on the right hand side was derived from Eq. (SA1). The second term is the static error which results from intrinsic noise in the imaging setup. ε is the resolution of the particle tracking algorithm, in practice $\approx$ 1/15 times the spatial resolution. For our imaging setup, the spatial resolution is $\approx .127 \mu m/pixel$, yielding a static error of $\approx 2*(.0667*0.127)^2 = .000143\mu m^2$. In all the data presented, we have subtracted off the static error, and only consider the remaining dynamic error.

The dynamic error results in a downward curvature in the MSD, typically most apparent at short lag times, as shown in (Figure SA.1) where the open circles are data for 1 μm diameter particles in water with $\sigma = 1/30 s$.. We have plotted the lag time rescaled MSD $\langle \Delta x^2(\tau) \rangle / 2\tau$ as a function of τ, in order to highlight this downward curvature. In the absence of dynamic error, the data should be a flat line with y-intercept D. The solid line is a fit to Eq. (SA2) from which we extract $D = .512\,\mu m^2/s$ as expected for a 1 μm diameter particle diffusing at T = 298 K with $\eta = 1\,mPa\,s$. Once D is extracted, the dynamic error can be completely removed by adding $2D\sigma/3$ to the MSD data, and the expected flat line is recovered, as the solid circles in Figure SA.1 attest.

This procedure can be generalized to arbitrary functional forms of the MSD: $f(\tau,\mathbf{x})$ where $\mathbf{x}$ includes all model parameters. First, $f(\tau,\mathbf{x})$ is convolved with instrumental resolution to yield $f(\tau,\mathbf{x},\sigma)$ which can then be fitted to the dynamic error-biased experimental data to extract $\mathbf{x}$, the parameters for the unbiased MSD. Note that the derivation of $f(\tau,\mathbf{x},\sigma)$ does not incur the cost of introducing a new parameter; the value of σ is known. The dynamic error for each lag time $\delta(\tau)$

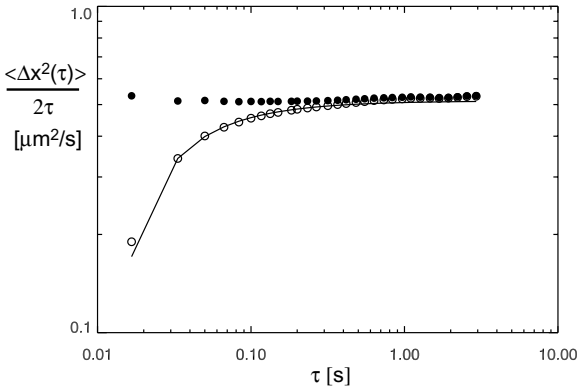

Figure SA.1: Scaled mean square displacement as a function of lag time for a 1 μm particle diffusing in water. Open circles are the msd obtained with $\sigma = 1/30s$ on the CCD camera. Solid line is a fit to Eq. (SA2) with $\sigma = 1/30s$ yielding $D = .512\mu m^2/s$ as expected for a 1 μm diameter particle diffusing at T = 298 K with $\eta = 1 mPa s$. Solid circles are the msd corrected for dynamic error as outlined in the text.

can then be estimated as $\delta(\tau) = |f(\tau,\mathbf{x}) - f(\tau,\mathbf{x},\sigma)|$. Once $\delta(\tau)$ is obtained, the dynamic error corrected MSD: $\langle\Delta x^2(\tau)\rangle = \langle\Delta x^2(\tau,\sigma)\rangle + \delta(\tau)$ can be obtained.

We use this procedure to correct our data. The first step is to find a suitable functional form to fit the MSD. With the exception of the earliest time data at t = 10 minutes, our MSDs are not linear, thus precluding the use of the Newtonian fluid model of Eq. (SA2). The next simplest form is a power law MSD: $\langle\Delta x^2(\tau)\rangle = A\tau^\alpha$. Plugging this form into Eq. (SA1) yields:

$$\langle\Delta x^2(\tau,\sigma)\rangle = A\sigma^\alpha \frac{\left(\frac{\tau}{\sigma}+1\right)^{2+\alpha} + \left(\frac{\tau}{\sigma}-1\right)^{2+\alpha} - 2\left(\frac{\tau}{\sigma}\right)^{2+\alpha} - 2}{(1+\alpha)(2+\alpha)} \tag{SA3}$$

which is Eq. (30) in Ref. (1). Eq.(SA3) described the t = 1 hr data well, shown in Figure SA.2.

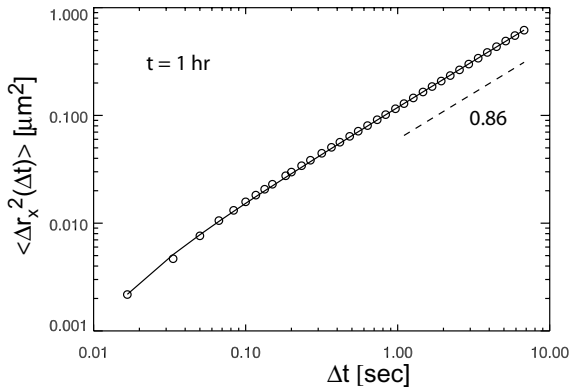

Figure SA.2: mean square displacement for t = 1 hr data. Solid line is a fit to Eq. (SA3)

However, the power law form did not work for $t \geq 2$ hr post-gel data, as shown in Figure SA.2. The poorness of the fits, particularly at the short lag times, indicates that the downward curvature cannot wholly be accounted for by dynamic error alone. Otherwise, we would have been able to obtain good fits of the MSDs with Eq. (SA3) as in the t = 1 hr data. Thus, the downward curvature is a feature of the relaxation of the gel network.

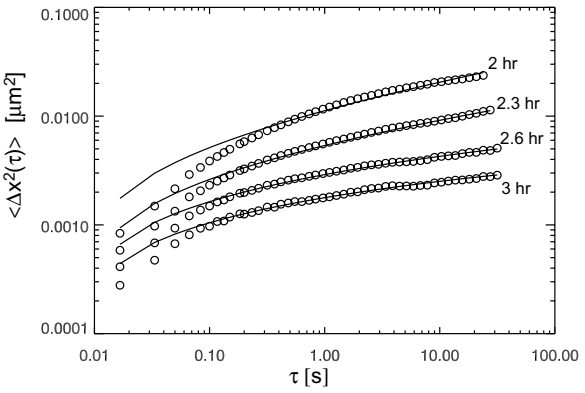

Figure SA.3: Post-gel MSD data (circles) along with the best fit (lines) to Eq. (SA3).

A natural choice to describe the tracer MSD expected for a gel would be the Voigt model, considered in Eq. (22) of Ref. (1). However, we found that the single relaxation time exponential saturation described by the Voigt model was insufficient to capture the slow saturation of our data which grows as a weak power law over our entire experimental time window. Moreover, we have a further constraint due to scaling considerations: the functional form for the data must be consistent with collapse under time-cure superposition scaling (i.e. $f(G,\omega) = (G/G_0)f(\omega/\omega_0)$). The simplest functional form that described the behavior of our data well was the empirical form: $\langle \Delta x^2(\tau) \rangle = Aln(1+\tau/\tau_0)$. Note that this form is not expected to be the true form since gels must saturate at long times and the logarithm does not, but it is good over the dynamic range of our data. Plugging into Eq.(SA1) yields:

$$\langle \Delta x^2(\tau,\sigma)\rangle = \frac{A\tau_0}{\sigma} - \frac{A}{2}\left(\frac{\tau+\tau_0}{\sigma}-1\right)^2 ln(\tau+\tau_0) + A\left[\frac{1}{2} - \left(\frac{\tau+\tau_0}{\sigma}\right)\left(1+\frac{\tau+\tau_0}{2\sigma}\right)\right] ln\left(1+\frac{\tau}{\tau_0}\right) + \frac{A}{2}\left(\frac{\tau+\tau_0}{\sigma}-1\right)^2 ln(\tau+\tau_0-\sigma) - A\left(1+\frac{\tau_0}{\sigma}\right)^2 ln\left(1+\frac{\sigma}{\tau_0}\right) + \frac{A}{2}\left(1+\frac{\tau+\tau_0}{\sigma}\right)^2 ln\left(1+\frac{\tau+\sigma}{\tau_0}\right). \quad \text{(SA4)}$$

We find a good fit for the post-gel data using Eq. (SA4), as shown in Figure SA.4.

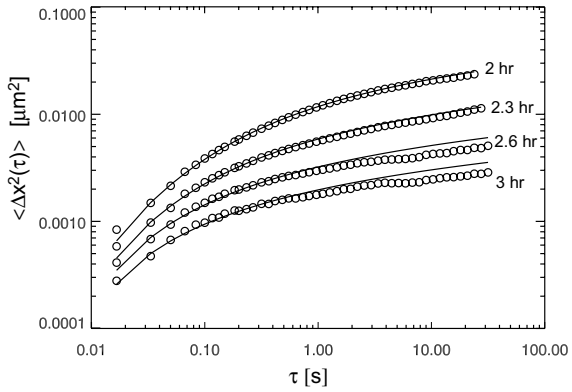

Figure SA.4: Post-gel MSD data (circles) along with the best fit (lines) to Eq. (SA4).

Using Eq.(SA2) for t = 10 min, Eq. (SA3) for t = 1 hr, and Eq. (SA4) for $t \geq 2hr$, we are able to correct for the dynamic errors in all our MSD data. In Figure SA.5 we show the results of the correction. The solid line is the dynamic error-biased data and the dashed lines are the data after their respective corrections have been made. For the $t \leq 1hr$ data, the downward curvature has been largely eliminated, confirming that it was an artifact of dynamic error. For the $t \geq 2hr$ data, however, the downward curvature persists, indicating that it is a feature of the relaxation dynamics of the SWNT gel.

The dynamic error corrected MSDs, denoted by the dashed lines in the figure, are exhibited in Fig. 1 of the main text and is used to calculate the viscoelastic moduli exhibited in Figs. 2 and 3. Comparing the moduli obtained with the dynamic error-biased data and without in Figure SA.6,

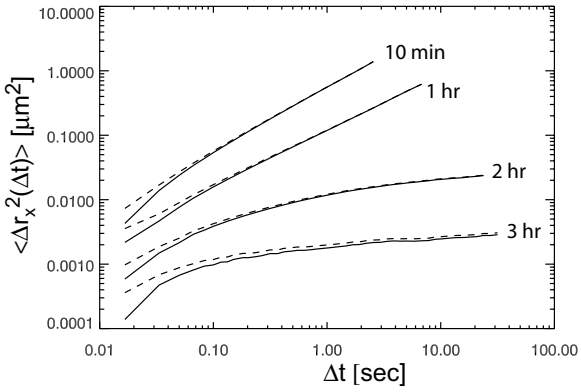

Figure SA.5: mean square displacement for t = 10 min, 1hr, 2hr, and 3 hr. Solid lines are the uncorrected MSD. Dashed lines are the dynamic error corrected MSD.

indicates that dynamic error can shift the crossover of the moduli and tends to affect the viscous modulus to a greater extent than the storage modulus in our post-gel data.

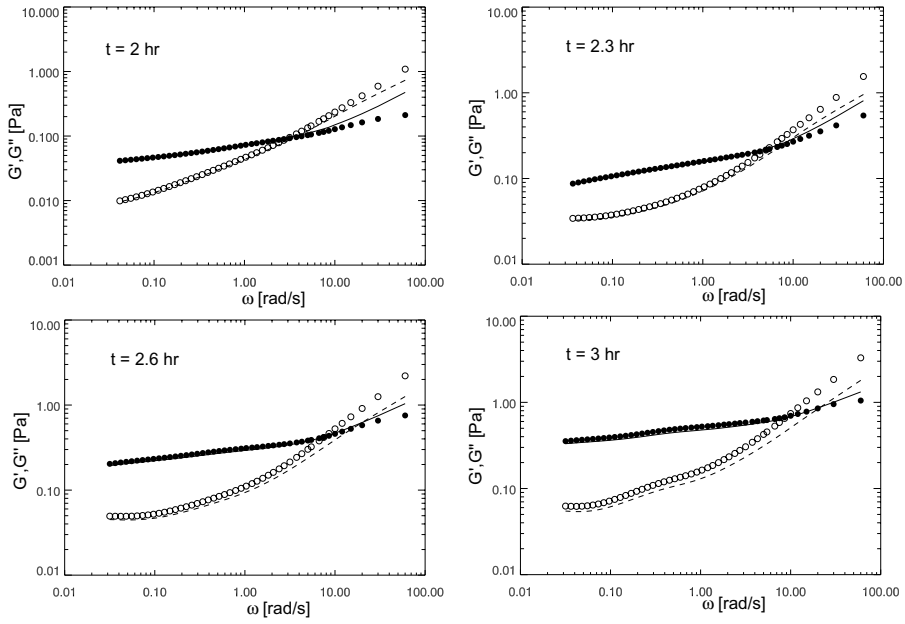

Figure SA.6: Viscoelastic moduli derived from the MSD for gel times above the percolation transition. G' and G" derived from dynamic error-biased MSD data are solid and open circles respectively. Solid and dashed lines are the G' and G", respectively, derived from the dynamic error corrected MSD.

The dynamic error corrected $G^*(\omega)$ data denoted by the solid and dashed lines is exhibited in Figs. 2,3, and 8 of the main text.

In this section of the Supporting information, we provide a detailed derivation of Eq. (1) in the main text. We begin by considering the crossing probability of two rods with length L and center-to-center separation S. Both rods can assume any orientation in 3-dimensional space, and the boundary of possible orientations delimits a sphere of diameter L around each rod center. Clearly, the separation between rod centers must be less than the length of the rods, i.e., $S < L$, in order for them to potentially cross, as illustrated in Figure SB.1A. There are two cases of interest: (i) $0 < S < L/2$ and (ii) $L/2 < S < L$. When (i) is satisfied, the centers of both rods are in the overlap region, regardless of their angular orientations. Therefore, the probability of overlap is one. When (ii) is satisfied, the two spheres will overlap, and the solid angle Ω subtending their overlap region is directly proportional to the fraction of possible angular orientations that each rod can assume whilst having a non-zero probability of overlapping the other rod. In turn, the probability of overlap P_{over} is just the product of the probabilities of each rod having the same angular restriction. Thus, having both rods in the overlap region is proportional to the square of the solid angle subtended by the overlap region:

$$P_{over} \propto \left(\frac{\Omega}{4\pi}\right)^2 = \frac{1}{(4\pi)^2}\left[\frac{4\pi L(L-S)}{L^2}\right]^2 = \left(1-\frac{S}{L}\right)^2. \tag{SB1}$$

Taken together, the probability of overlap for the two cases is:

$$P_{over} = \begin{cases} 1 & \text{if } \ 0 < S < \frac{L}{2} \quad (i) \\ 4\times(1-\frac{S}{L})^2 & \text{if } \ \frac{L}{2} < S < L \quad (ii) \end{cases} \tag{SB2}$$

Having both rods in the overlap region is a necessary but not sufficient condition to guarantee contact. There is an additional probability P_{ang} which depends on the relative angular orientations of the rods. The probability of crossing is given by $P_{cross} = P_{over} \times P_{ang}$. When both rods are in the overlap region, let the angle between rod 2 and the axis connecting two rod centers to be α, as shown in Figure SB.1B. The probability of rod 2 crossing rod 1 is proportional to the angle β subtending the projection of rod 2 onto the sphere of rod 1. Considering rotational symmetry with

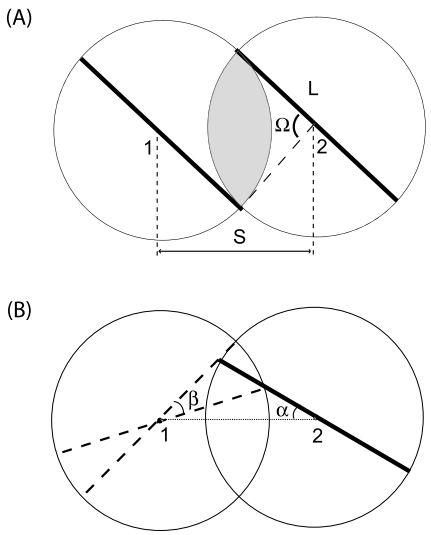

Figure SB.1: (A) Geometry of crossing probability of 2 rods of length L separated by distance S. Shaded region is overlap of the rod's spheres of possible angular orientation. Ω is the solid angle subtended by the overlap region. (B) Angles of possible intersections. β is the angular range of rod 1 that will cross rod 2 given rod 2 forms an angle α with respect to the separation axis.

respect to the axis connecting the centers of rods 1 and 2, and the fact that the diameter of the rods $\sigma << L$, P_{ang} is:

$$P_{ang} = \begin{cases} \int_0^{\pi/2} \frac{\beta(\alpha,\frac{S}{L})2\sigma L}{\pi L^2} \frac{\pi L^2 sin\alpha}{\pi L^2} d\alpha & \text{if } \ 0 < S < \frac{L}{2} \quad (i) \\ \int_0^{\theta} \frac{\beta(\alpha,\frac{S}{L})2\sigma L}{\pi L(L-S)} \frac{\pi L^2 sin\alpha}{4\pi L(L-S)} d\alpha & \text{if } \ \frac{L}{2} < S < L \quad (ii) \end{cases} \tag{SB3}$$

where for case (ii), θ is the largest angle that rod 2 can adopt whilst making contact with the sphere of rod 1. For case (ii), the angle breaks down into two subcases (iia) $\frac{L}{2} < S < \frac{L}{\sqrt{2}}$ and (iib) $\frac{L}{\sqrt{2}} < S < L$:

$$\theta = \begin{cases} \arcsin(\frac{L}{2S}) & \text{if } \ \frac{L}{2} < S < \frac{L}{\sqrt{2}} \quad (iia) \\ \arccos(\frac{S}{L}) & \text{if } \ \frac{L}{\sqrt{2}} < S < L \quad (iib) \end{cases} \tag{SB4}$$

Therefore, P_{cross} of two rods with length L and separation S is:

$$P_{cross} = P_{over} \times P_{ang} = \frac{\sigma}{L} I\left(\frac{S}{L}\right) \tag{SB5}$$

where $I(\frac{S}{L}) = \frac{2}{\pi}\int_0^{\{\frac{\pi}{2},\theta\}} \beta(\alpha,\frac{S}{L})\sin\alpha\, d\alpha$ for cases (i) and (ii) respectively.

Now consider the number of contacts or crosses one rod can have with other rods in its vicinity. Let the rod number density to be $n = \frac{N_{rod}}{V}$, where N_{rod} is the total number of rods and V is the volume of the gel. The mean number of contacts per rod, $\overline{N}_{c,1}$, is

$$\begin{aligned}\overline{N}_{c,1} &= \int P_{cross} n dv \\ &= \int \frac{\sigma}{L} I\left(\frac{S}{L}\right) n dv \\ &= \frac{4\pi n\sigma}{L}\int_0^L I\left(\frac{S}{L}\right) S^2 dS \\ &= 4\pi n L^2 \sigma \int_0^1 I(x) x^2 dx. \end{aligned} \tag{SB6}$$

The contact density thus is

$$\begin{aligned}\frac{N_c}{V} &= \frac{N_{rod}\times\overline{N}_{c,1}}{V} \\ &= 4\pi J \frac{L^2\sigma N_{rod}^2}{V^2} \sim \phi^2 \end{aligned} \tag{SB7}$$

where J=$\int_0^1 I(x)x^2dx$=0.0403, and this is Eq. (1) in the main text. The J obtained from simulation data is 0.11. The discrepancy between simulation and numerical evaluation of the integral is due to an underestimate of solid angles when α is very small.

References

(1) Savin, T.; Doyle,P.S. *Biophys. J.* **2005**, 88(1), 623-638.